Spatial and temporal dynamics in eddy covariance observations of methane fluxes at a tundra site in Northeastern Siberia

Parmentier, F.J.W.; van Huissteden, J.; van der Molen, M.K.; Schaepman-Strub, G.; Karsanaev, S.A.; Maximov, T.C.; Dolman, A.J.

published in
Journal of Geophysical Research
2011

DOI (link to publisher)
10.1029/2010JG001637

document version
Publisher's PDF, also known as Version of record

Spatial and temporal dynamics in eddy covariance observations of methane fluxes at a tundra site in northeastern Siberia

F. J. W. Parmentier,[1,2] J. van Huissteden,[1] M. K. van der Molen,[3] G. Schaepman-Strub,[4] S. A. Karsanaev,[5] T. C. Maximov,[5] and A. J. Dolman[1]

Received 22 December 2010; revised 12 April 2011; accepted 2 May 2011; published 4 August 2011.

[1] In the past two decades, the eddy covariance technique has been used for an increasing number of methane flux studies at an ecosystem scale. Previously, most of these studies used a closed path setup with a tunable diode laser spectrometer (TDL). Although this method worked well, the TDL has to be calibrated regularly and cooled with liquid nitrogen or a cryogenic system, which limits its use in remote areas. Recently, a new closed path technique has been introduced that uses off-axis integrated cavity output spectroscopy that does not require regular calibration or liquid nitrogen to operate and can thus be applied in remote areas. In the summer of 2008 and 2009, this eddy covariance technique was used to study methane fluxes from a tundra site in northeastern Siberia. The measured emissions showed to be very dependent on the fetch area, due to a large contrast in dry and wet vegetation in between wind directions. Furthermore, the observed short- and long-term variation of methane fluxes could be readily explained with a nonlinear model that used relationships with atmospheric stability, soil temperature, and water level. This model was subsequently extended to fieldwork periods preceding the eddy covariance setup and applied to evaluate a spatially integrated flux. The model result showed that average fluxes were 56.5, 48.7, and 30.4 nmol CH_4 m^{-2} s^{-1} for the summers of 2007 to 2009. While previous models of the same type were only applicable to daily averages, the method described can be used on a much higher temporal resolution, making it suitable for gap filling. Furthermore, by partitioning the measured fluxes along wind direction, this model can also be used in areas with nonuniform terrain but nonetheless provide spatially integrated fluxes.

Citation: Parmentier, F. J. W., J. van Huissteden, M. K. van der Molen, A. J. Dolman, G. Schaepman-Strub, S. A. Karsanaev, and T. C. Maximov (2011), Spatial and temporal dynamics in eddy covariance observations of methane fluxes at a tundra site in northeastern Siberia, *J. Geophys. Res.*, *116*, G03016, doi:10.1029/2010JG001637.

1. Introduction

[2] Methane emissions from Arctic ecosystems play a special role in the global carbon cycle due to the amplified and unprecedented warming of the region [*Serreze et al.*, 2000; *Kaufman et al.*, 2009] in combination with the large expected temperature sensitivity of the carbon stores in permafrost areas [*Christensen et al.*, 2004]. It has been suggested that this combination could lead to a positive feedback when higher temperatures lead to more carbon availability through increased melting of the permafrost which would lead, in turn, to higher methane emissions, resulting in increasingly higher temperatures [*Oechel et al.*, 1993; *McGuire et al.*, 2009]. Therefore, to better understand the relationships of these emissions to environmental parameters, methane fluxes have been measured in the past two decades at a number of sites using chamber flux measurements [*Christensen et al.*, 1995; *van Huissteden et al.*, 2005], and, since recently, the eddy covariance technique [*Friborg et al.*, 2000; *Wille et al.*, 2008].

[3] Most of these studies on methane emissions preferred chamber flux measurements for a number of reasons. For example, the chamber flux method has a low power requirement, which makes it applicable in remote areas where a steady power supply is absent. Also, due to the small footprint, correlations between environmental parameters such as soil temperature, water level and vegetation are more easily determined. Furthermore, chamber flux measurements are portable and therefore measurements can be readily performed at a relatively large number of locations [*Christensen et al.*, 1995; *van Huissteden et al.*, 2005].

[1]Department of Hydrology and Geo-environmental Sciences, Faculty of Earth and Life Sciences, VU University Amsterdam, Amsterdam, Netherlands.
[2]Division of Physical Geography and Ecosystems Analysis, Department of Earth and Ecosystem Sciences, Lund University, Lund, Sweden.
[3]Meteorology and Air Quality Group, Wageningen University, Wageningen, Netherlands.
[4]Institute of Evolutionary Biology and Environmental Studies, University of Zürich, Zurich, Switzerland.
[5]BioGeochemical Cycles of Permafrost Ecosystems Lab, Institute for Biological Problems of the Cryolithozone SB RAS, Yakutsk, Russia.

0148-0227/11/2010JG001637

[4] On the other hand, chamber flux measurements are very labor intensive, have a low temporal resolution and can easily be disturbed by the person performing the measurement. Most of these concerns can be alleviated by the use of automatic flux chambers, since they perform measurements at a regular interval with much less effort [*Mastepanov et al.*, 2008]. However, with automatic chambers the drawbacks that are inherent to point measurements remain. For example, when flux chamber measurements are being upscaled to an integrated flux estimate of a larger area, a significant amount of measurements are needed for each vegetation type present, together with a precise vegetation mapping [*van der Molen et al.*, 2007]. The higher number of measurements involved all have their own added uncertainty, making it more complicated to establish a correctly upscaled flux. Besides, even if very precise measurements are performed and the vegetation has been mapped in close detail, the fact remains that chamber measurements decouple the surface from atmospheric influences such as wind and turbulence and they are unsuitable for registering irregular events such as ebullition, all of which can have a significant effect on the amplitude of fluxes, methane in particular [*Kellner et al.*, 2006; *Sachs et al.*, 2008].

[5] Therefore, to be able to measure methane fluxes in a nonintrusive way, over large terrain and with a high temporal resolution, the eddy covariance method may perform better. This method has already been well established for the measurement of evaporation and CO_2 fluxes [*Aubinet et al.*, 2000; *Moncrieff et al.*, 1997] and has been successfully applied to measure methane fluxes as well. For example, one of the earliest studies on eddy covariance of methane fluxes was performed by *Fan et al.* [1992], who used a fast response flame ionization detector and a prototype fast HeNe laser methane monitor to measure methane emissions from tundra in southwestern Alaska and found relationships with wind speed for methane emissions from lakes. Alternatively, *Verma et al.* [1992] measured methane fluxes in a Minnesota peatland with a fast response tunable diode laser spectrometer (TDL) [*Zahniser et al.*, 1995] and found the method to be satisfactory for measuring methane fluxes. Afterward, this method was used in several other eddy covariance studies. For example, *Suyker et al.* [1996] measured methane fluxes in a fen in central Saskatchewan and could model observed fluxes from nonlinear relationships with midday temperature measurements and water level. *Friborg et al.* [2000] expanded upon this model, with measurements obtained at a high Arctic site in NE Greenland, by using daily averages and by adding relationships with active layer depth. *Wille et al.* [2008] applied a similar nonlinear model, explaining most day to day variation by relationships with soil temperature and friction velocity, to measurements obtained with a TDL from polygonal tundra on a northeastern Siberian site in the delta of the Lena river. *Sachs et al.* [2008], with measurements at the same site but in a later year, further developed the model by adding air pressure, which significantly improved results. Also, it was shown that the model performed well over the entire growing season.

[6] Most of these eddy covariance studies used TDL devices that had the large drawback that they had to be cooled (either with liquid nitrogen or a cryogenic system) and required regular (daily or subdaily) calibration to obtain precise measurements of methane concentrations. Recently, an off-axis integrated cavity output spectroscopy method was introduced that can measure methane concentrations at a high frequency (10 Hz) and it was shown to give good results when used for eddy covariance [*Hendriks et al.*, 2008; *Zona et al.*, 2009]. Although this application requires a large pump, to pass air at sufficient speed through the system, and power requirements therefore remain high, this method does not require cooling or regular calibration. In areas where liquid nitrogen and calibration gases are not readily available, this method opens up new measurement opportunities, given a steady power supply.

[7] When considering new study areas, it becomes apparent that most previous studies on Arctic carbon cycling have been performed in Alaska, Canada or Scandinavia [*Whalen and Reeburgh*, 1990; *Fan et al.*, 1992; *Morrissey et al.*, 1993; *Torn and Chapin*, 1993; *Vourlitis and Oechel*, 1997; *Oechel et al.*, 1998; *Christensen et al.*, 2004; *Schuur et al.*, 2008; *Dorrepaal et al.*, 2009] and only few in Siberia [*Christensen et al.*, 1995; *Nakano et al.*, 2000; *Corradi et al.*, 2005; *van der Molen et al.*, 2007; *Kutzbach et al.*, 2007], while the largest extent of the Arctic lies in Russian territory. Moreover, these are largely studies using flux chambers, not eddy covariance.

[8] In 2003, to fill this gap in our knowledge of carbon cycling around the arctic, a new station was established in northeastern Siberia to measure fluxes of CO_2 and CH_4. While CO_2 fluxes have been measured with eddy covariance from the beginning, measurements of methane fluxes had to be performed with the flux chamber method, because of the remoteness of this area and the associated logistical difficulties. As mentioned earlier, measurements with this method can be difficult to translate to a larger area and therefore the new off-axis spectroscopy method was used to determine spatially integrated methane emissions at this site in the summer of 2008 and 2009. In this paper, we show the results and analysis of these measurements with the help of the aforementioned model framework [*Suyker et al.*, 1996; *Friborg et al.*, 2000; *Wille et al.*, 2008; *Sachs et al.*, 2008]. Previous studies using this framework considered nonlinear relationships to daily averages, while this new study found that fluxes could be well described on a 3 h interval. This was achieved by including the attenuating effect of atmospheric stability on flux measurements, while production was related to soil temperature and water level. This result largely improves the temporal scale of the model framework, making it suitable for gap filling. Furthermore, the relationships found were applied to simulate spatially integrated methane fluxes in the highly heterogenous terrain of the study site, a common trait of most tundra sites.

2. Materials and Methods

2.1. Site Description

[9] The research site (70°49′44.9″N, 147°29′39.4″E) is located approximately 30 km to the northwest of the settlement of Chokurdakh in the nature reserve "Kytalyk" in northeastern Siberia, alongside the river Berelekekh (Yelon), a tributary to the Indigirka (as shown in Figure 1). At a considerable distance from the river, the eddy covariance tower is situated in a depression that originated as a thermokarst lake of Holocene age that has been drained by fluvial erosion.

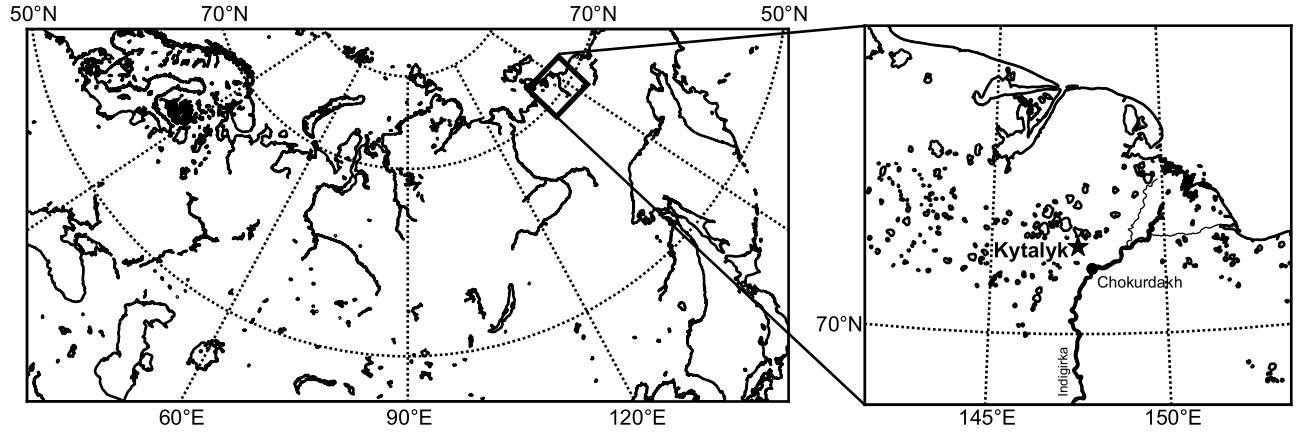

Figure 1. The location of the research site within northeastern Siberia.

[10] The climate at the site is continental, with an average temperature of −10.5°C and typical temperatures of −25 to −40°C in winter and 5 to 25°C in summer. Normally snowmelt starts at the end of May, early June. Apart from some isolated patches, usually most of the snow is melted by the first half of June. Bud break occurs somewhat later at the end of June or start of July, together with the first truly warm days of the year. However, temperatures vary rapidly in summer when either cold winds are blowing from the Arctic Ocean to the north (~100 km) or warm winds from the Siberian continent to the south. At the start of September, when temperatures again drop below zero, the growing season stops. By then, the growing season will have seen half of the yearly precipitation as rain while the other half falls as snow in the rest of the year. Snow cover is around 30 cm with little variation in recent years. Total precipitation is around 220 mm per year and while this is a relatively low amount compared to other parts of the world, most evaporation is limited to the short growing season and as such soil conditions remain wet.

[11] Because of the cold climate, the area is underlain by permafrost and areas with a well developed polygonal structure as well as areas with small palsa-like hills occur. These cryogenic structures have led to shallow elevation differences in the landscape with dryer areas where ice lenses created slightly higher lying mounds and wetter, mostly flooded, areas in between these raised areas. In the wet areas, the soil is overlain by a coarse peaty organic top layer of around 10 to 15 cm, consisting of sedge roots and/or Sphagnum peat, while drier parts have a less developed organic layer. A difference also exists in active layer depth, which varies from 40 to 50 cm in the wetter parts to 20 to 30 cm in the dryer parts. Furthermore, in areas where ice wedges are actively developing, open water and small ponds occur. These ponds cover 5% in the west of the research area, locally up to 10%, while the northeast part almost completely lacks ponds.

[12] These small-scale hydrological changes influence the vegetation composition. In dry areas, vegetation consists of *Betula nana* and *Salix pulchra* dwarf shrubs or hummocks of the sedge *Eriophorum vaginatum* with *Salix pulchra* in between. In these areas a moss and lichen ground cover is common. This dry vegetation type occurs on well drained slopes, palsas and on the rims of ice wedge polygons. In the transition zone from a dry to a wet area, mosses and lichens are replaced by *Sphagnum* spp. and shrub cover is largely reduced. In these parts, *Potentilla palustris* occurs and sedge cover increases to 50% with species such as *Arctagrostis latifolia*, *Eriophorum angustifolium* and *Carex aquatilis*. These last two species dominate the wet, flooded parts of terrain depressions and polygon centers where *Sphagnum* is absent and sedge cover is around 80 to 100%. A more detailed description of the studied area is given by *van der Molen et al.* [2007].

2.2. Instrumentation

[13] The equipment used, measured a large set of environmental parameters. To measure wind speeds and temperature, an ultrasonic anemometer (Gill Instruments, Lymington, UK, type R3-50) was installed on top of a small mast at a height of 4.7 m. At the same height, with a separation of 20 cm, an inlet was situated where air was drawn down toward the fast methane analyzer (Los Gatos Research, Mountain View, California, USA, type DLT-100). This inlet was fitted with a filter, which had a pore size of 60 μm, to prevent dust or insects from entering the system. To prevent rainwater from entering the system, a metal cap was placed over the filter and the air was first led upward for 30 cm through a 3/8″ metal tube and back downward following a U-turn. At a height of 3 meters and below, the air was led through flexible silicon tubing, with the same internal diameter, toward the box in which the fast methane analyzer was situated. At the end of the setup, a dry vacuum scroll pump (XDS35i, BOC Edwards, Crawly, UK) was installed that drew air through the system, which was exhausted through a silencer. Although this pump is capable of speeds up to 9.72 10^{-3} m^3 s^{-1}, the pressure in the measurement cell should be maintained at 210 hPa during operation and as such the actual pumping speed was 5.5 10^{-3} m^3 s^{-1}. With a measurement cell volume of 0.55 m^3, this provided the system with an effective instrument response time of 0.1 s.

[14] Because the vacuum scroll pump and the fast methane analyzer had a high power requirement, a diesel generator was set up 150 m south of the tower to provide power. The generator required refueling twice a day and as a consequence CH_4 measurements were constrained to the period that the research station was occupied. All other measurements, including the sonic anemometer, could run autonomously

with a power supply from solar panels and a small wind generator. The data put out by the system was logged at a frequency of 10 Hz to a handheld computer [*van der Molen et al.*, 2006] and half-hourly fluxes were computed afterward following the Euroflux methodology [*Aubinet et al.*, 2000], with the addition of an angle of attack-dependent calibration [*van der Molen et al.*, 2004; *Nakai et al.*, 2006]. Corrections were applied for the time lag of 0.6 s between the sonic anemometer and the measurement cell and for the damping effect caused by the instrument response time [*Moore*, 1986]. Corrections for density fluctuations according to *Webb et al.* [1980] were not applied since the flow of air through the tube dampened density fluctuations and corrections for water vapor fluctuations were found to be very small, as was also found by *Zona et al.* [2009] with a similar methane analyzer. As a final check, it was found that the energy balance for the measured period showed the same closure as reported earlier by *van der Molen et al.* [2007], who found a good 1:1 agreement at the same site but for previous years. A more detailed study on the performance of the DLT-100 methane analyzer has been performed by *Hendriks et al.* [2008] for a site in the Netherlands with largely identical instrumentation.

[15] In the summer of 2008, the fast methane analyzer was set up for the first time. Due to logistical difficulties however, measurements could not start before 25 July. From that day on, measurements were performed until 9 August, when the field campaign ended. On 28 July, a generator failure caused the system to be offline for approximately 15 h but, apart from that brief period, measurements were continuous. In 2009, the measurements were started on 5 July, at the beginning of the field campaign, after which measurements continued uninterrupted until 3 August.

[16] In another tower, situated 5 meters away from the eddy covariance tower, a shortwave radiometer (Kipp & Zn, Delft, the Netherlands, type albedometer, CM7b), up- and down-facing longwave radiometers (The Eppley Laboratory, Newport, RI, USA, type PIR) and a net radiometer (Campbell Scientific, Logan, UT, USA, type Q7) were installed. Soil temperature sensors (type Pb107, manufactured at the VU University Amsterdam) were installed in two profiles, each reaching 60 cm into the ground and measuring temperature at 10 depths each. One profile was situated in an inundated depression with vegetation dominated by sedges, while the other was situated in a higher, drier part dominated by shrubs. A pressure sensor (manufactured at the VU University Amsterdam) was used to measure barometric pressure, while a tipping bucket rain gauge (Campbell Scientific, Logan, UT, USA) was used to measure precipitation. Each day, water level was measured manually from a piezometer that was installed into the soil of the low part of the polygon, where the water level remained above the surface for the measured period. Although significant differences in water level exist throughout the area, it was found that variations in the water level at this single measurement point represented fluctuations in the water table at a larger scale. Manual measurements that were performed throughout the area showed the same day to day variation and as such water level measurements at this one point are a reasonable indication for water level changes in the area around the tower.

2.3. Chamber Measurements and Upscaling

[17] During the field work campaigns of 2007, 2008 and 2009, independent methane flux measurements were performed with manual flux chambers that were connected to an INNOVA 1412 Photoacoustic field Gas-monitor (LumaSense Technologies A/S, Ballerup, Denmark) following the same measurement practice as described by *van Huissteden et al.* [2005]. At varying dates and during daytime, measurements were performed on 20 different locations that covered the main vegetation types at the site and the variability therein. Together with each measurement, active layer depth was measured by inserting a steel rod into the ground until it hit the permafrost, noting the distance between the surface and the permafrost. This allowed for a spatially integrated value of this parameter.

[18] To be able to compare the flux chamber measurements to the eddy covariance, these were upscaled with the use of a satellite-derived vegetation map. To obtain this map, extensive ground truth on vegetation composition was collected in July 2008 and 2010. In 31 georeferenced validation plots of 20×20 m, species composition was determined at 12 locations. Based on the recorded dominant species, the 31 validation plots were then grouped into 5 vegetation communities. All validation plots per vegetation community were used as training areas for a supervised classification. A maximum likelihood classification algorithm (implemented in ENVI) was applied on an atmospherically corrected GeoEye-1 satellite image that was acquired on 19 August 2010. GeoEye-1 provides a spatial resolution of 2 m for the multispectral bands (blue: 480 nm, green: 545 nm, red: 672.5 nm, nir: 850 nm). Including all classes in the confusion matrix, the overall accuracy of the resulting vegetation map was 86.79% and the kappa coefficient 0.75. This classification was then applied to a 300 m diameter around the flux tower to establish a vegetation map. By multiplying the average methane flux per vegetation class with its fractional cover and summing the results, an average methane flux for the area could be determined.

2.4. Flux Model

[19] The model used in this study was developed from previous studies on eddy covariance measurements of methane that noted that observed fluxes could be best described by nonlinear relationships with a varying set of environmental parameters [*Suyker et al.*, 1996; *Friborg et al.*, 2000; *Wille et al.*, 2008; *Sachs et al.*, 2008]. Parameters such as temperature, water level and/or friction velocity were related to daily averages of fluxes and as such most variation could be explained. In this study, production of methane was related to both water level and soil temperature but it was less practical to compare these parameters to daily averages of the measured methane flux. At the study site, large differences in wetness and vegetation composition, and thus methane emissions, exist within the area [*van der Molen et al.*, 2007]. As the wind direction changes, the footprint of the tower and the amplitude of the measured methane flux change. Therefore, the temporal resolution of the model has to be high enough to appreciate the contributions from different wind directions separately. A consequence of this shorter averaging period is that the diurnal variation in environmental parameters that influence the measured flux have to be captured as well. It was found after initial testing that 3-hourly averages

would both be short enough to capture most changes in wind direction and would also capture diurnal patterns in other environmental parameters sufficiently.

[20] One environmental parameter that shows a clear diurnal pattern, is atmospheric stability. While atmospheric stability does not affect the bacterial production of methane within the soil, stable atmospheric conditions can have a suppressing effect on the transport of trace gases [*Hollinger et al.*, 1998]. During stable atmospheric conditions, usually during nighttime when air close to the ground is cooler and more dense, vertical transport of air parcels, including methane, is suppressed. During unstable atmospheric conditions, normally during daytime when air closer to the ground is warmer and less dense, vertical transport is stronger due to the enhanced buoyancy [*Denmead*, 2008]. If merely daily averages of methane flux are considered, the effect of atmospheric stability is averaged out but in the higher temporal resolution of the model in this study, these effects have to be taken into account.

[21] To calculate atmospheric stability, we used the stability function to the Monin-Obukhov length, L, according to *Paulson* [1970] for unstable ($L < 0$) and stable ($L > 0$) conditions as described in equation (1).

$$\Phi(L > 0) = (1 - 16(z/L))^{-1/2}$$
$$\Phi(L < 0) = 1 - 5(z/L) \quad (1)$$

Here z is the observation height minus the displacement height. This function was preferred over z/L itself, since it constrains outliers in the value of L, which could otherwise easily disturb model optimization. As a consequence, unstable conditions are expressed in the range $0 < \Phi < 1$, neutral conditions occur at $\Phi = 1$ and unstable conditions are expressed for values of $\Phi > 1$.

[22] In equation (2) it is shown how the observed methane flux is described with the use of the atmospheric stability function, soil temperature and water level.

$$F_{CH_4,model} = p_0 \cdot p_1^{\left(\Phi - \overline{\Phi}\right)} \cdot p_2^{\left(\left(T_{soil} - \overline{T_{soil}}\right)/10\right)} \cdot p_3^{\left(w_l - \overline{w_l}\right)} \quad (2)$$

Here, F_{CH_4} is the methane flux expressed in nmol m^{-2} s^{-1}, Φ is the result of the atmospheric stability function, T_{soil} is the soil temperature from an inundated area dominated by sedges (averaged for depths of 2 and 4 cm) in °C, w_l is the measured water level in cm, and p_0 to p_3 are the parameters on which the model was optimized. This optimization was done with a nonlinear least squares fit according to the Levenberg-Marquardt algorithm [*Levenberg*, 1944] as included in the Open Source Scientific Tools for Python (SciPy). With the use of this algorithm, the values of p_0 to p_3 were varied until the sum of squares of the difference of the model and the observed values was reduced to a minimum. After the values of these model parameters had been established, the model was also run for the fieldwork period of 2007 and the first half of the fieldwork period in 2008, before the methane eddy covariance measurements were started.

3. Results

3.1. Environmental Conditions

[23] In Figure 2, the environmental conditions during the fieldwork periods of 2007, 2008 and 2009 have been plotted. In 2007, the fieldwork started with several warm days with air temperatures around 25°C on 10 July. Hereafter, temperatures dropped gradually until they reached 5°C in mid-July, which was accompanied by several days of rain. Within this period, water level rose from +5 cm above the surface until +15 cm and it stayed high for the remainder of the fieldwork. After this period, the air temperature rose to 20 to 25°C in the last week of July. At the start of August, the air temperature dropped to 10°C and this period was met with regular showers of a few mm. During the fieldwork period, the active layer was very deep, starting at an average of 30 cm until 40 cm at the end of the fieldwork period. In wet areas, depths up to 50 cm had been recorded. This was mainly due to a much earlier start of the growing season, with snowmelt in mid-May, while in 2008 and 2009 snowmelt did not occur until June.

[24] The field campaign in 2008 started on 9 July with air temperatures around 5 to 10°C during the day and just above zero at night. Over the course of a week, temperatures increased gradually to a maximum of 32°C on 18 July. After this exceptionally hot day, the wind turned north and temperatures dropped back to values of 15°C and decreased further to 5°C in the course of several days. At 25 July, when the eddy covariance measurements of methane were started, temperatures peaked around 15°C. Two days later, two separate rain storms passed on 27 and 28 July with an intensity of about 10 and 25 mm, respectively. Up to that moment, the water level near the tower had been dropping steadily from +10 cm above the surface at the start of the measurements, to +5 cm just before the rain storms. After the rain storms, the water level had risen to +15 cm in just 2 days and would not drop below +10 cm above the surface for the remainder of the field campaign. The days following the rainstorms were cold, with temperatures around 5°C until the beginning of August, when temperatures rose again, up to 25 degrees on 5 August, which was followed by a couple of days with temperatures around 15°C. The depth of the active layer was shallow at the start of the fieldwork, with an average of 5 cm, although depths in the wet methane producing parts could be as deep as 10 cm. Active layer depth increased gradually during the fieldwork with a depth of 30 cm at the end and depths of 40 cm in the wetter parts of the tundra.

[25] In 2009, measurements were started on 6 July and temperatures were varying between 5 and 15°C for two weeks, after which temperatures rose to 20°C on 18 and 19 July. Precipitation was low in this period (around 10 mm in total), with small showers occurring irregularly. On 20 July, temperature was down to 5°C again and after that continued to rise steadily until approximately 25 degrees on 27 July. After this day, a couple of showers occurred and temperatures dropped and would remain around 5 to 10°C for the rest of the period. Water level was very low during the measured period. At the start of the fieldwork, the water level was +4 cm above the surface and steadily decreased in time. Many areas in the tundra were much drier than in previous years with smaller ponds and significant areas with sedges falling dry, in areas where there was standing water in 2008. The water level as measured near the tower however, remained above the surface for the entire period. Active layer depth at the start of the fieldwork was shallow, at 5 cm, and remained low for the fieldwork period,

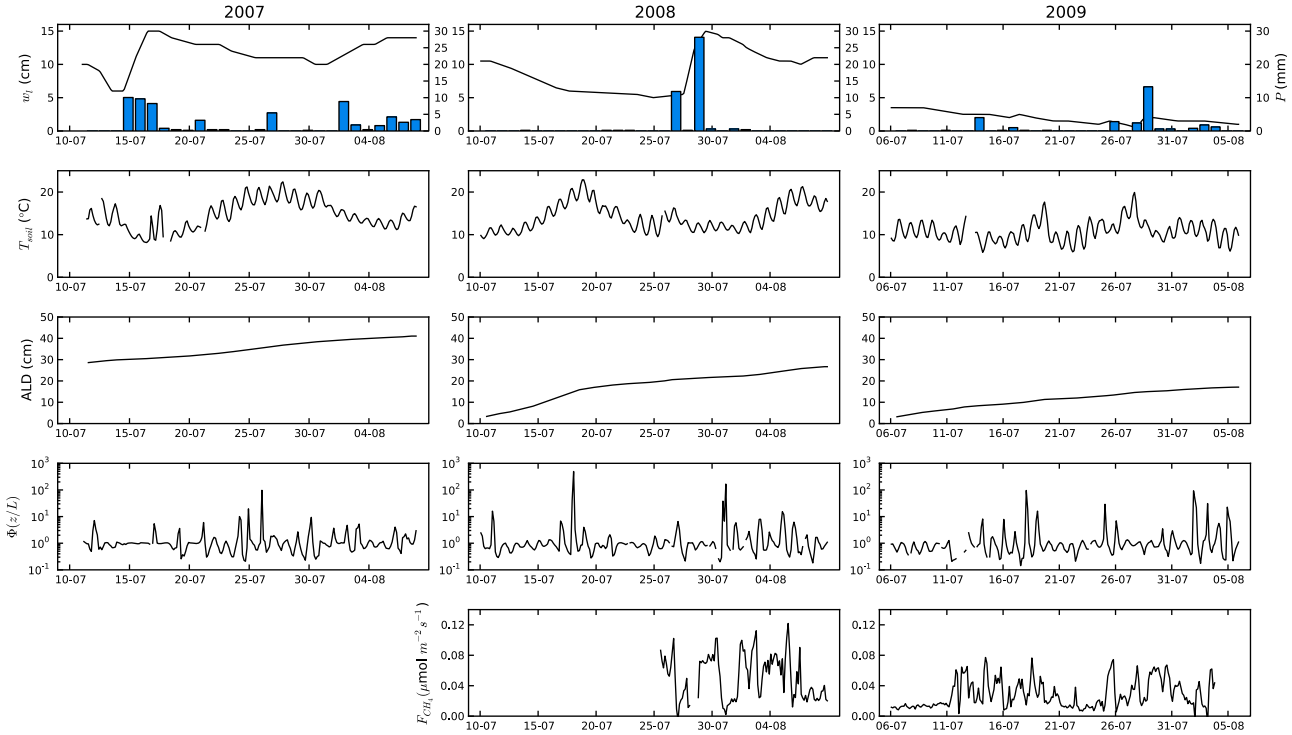

Figure 2. Environmental parameters measured during the 2008 and 2009 field campaigns. The top row shows water level in the piezometer near the tower, w_l, as a continuous line, while precipitation, P, is indicated by the blue bars. Soil temperature (averaged from a depth of 2 and 4 cm), T_{soil}, is shown in the second row. The third row shows the average active layer depth for the study area, and the fourth shows the results of the stability function, $\Phi(z/l)$. In the bottom row, the methane flux, F_{CH4}, has been plotted.

averaging around 20 cm at the start of August. In wet areas however, this depth could be as deep as 40 cm.

3.2. Methane Fluxes

[26] The observed fluxes, as shown in Figure 2, presented great variability. Within hours, fluxes changed by an order of magnitude. These changes coincided with a change in wind direction. When the wind was blowing from the northeast, fluxes were low. When the wind came from the south and west, fluxes were high. This partitioning can be explained by changes in the source area [*Jackowicz-Korczyński et al.*, 2010]. Figure 3 shows the area around the tower together with the satellite-derived vegetation map around the tower. In the center, the tower is shown while radially away from the tower the methane fluxes have been plotted in polar coordinates as a function of wind direction. This picture clearly shows that when the wind is coming from the northeast, fluxes are much lower.

[27] These different amplitudes can be explained by a difference in vegetation [*Bubier*, 1995]. In the background of Figure 3, the satellite-derived vegetation map is shown and for each sector the fractional vegetation cover is described in Table 1. Here it is shown that 63% of the "dry" sector is covered by a vegetation type that is associated with low to no methane fluxes, while 18% of the surface is covered by vegetation that emits high amounts of methane. Although the "mixed" sector is covered for 59% by dry vegetation types, the amount of vegetation that emits high to very high amounts of methane is much larger, up to 30%. In the "wet" sector, the amount of dry vegetation is clearly lower at 51% and the amount of vegetation emitting high amounts of methane is up to 32%, with a clear shift toward the vegetation type dominated by *Eriophorum angustifolium* and *Carex* sp., which show the highest emissions of all vegetation types.

[28] The amount of open water in the various sectors seems low but since most small ponds in the area have a similar size as the 2 m resolution of the multispectral satellite image, they are not always classified correctly. The same satellite picture was also available in the monochrome band, with a higher resolution of 0.5 m. From this picture a better assessment of the amount of small ponds (while ignoring the river) could be made and it was found that the dry and the mixed sector had 0.5% open water and the wet area 5%. This has been indicated in Table 1.

[29] To ascertain whether the size of the obtained vegetation map agreed with the source area of the tower, a footprint analysis was performed for the observed period according to the model presented by *Kormann and Meixner* [2001]. Typical dimensions of the footprint would be 100 to 200 m in width and 300 to 500 m in length, for an area that contributes 90% to the flux. Within this area, the highest relative contribution to the measured flux typically comes from an area around 30 to 50 meters away from the tower. When calculated for the radius of Figure 3, it was found that this area would contribute 75% to 90% of the flux. The size of the fetch did not show any relationship with wind direction and therefore these values are typical for all three sectors.

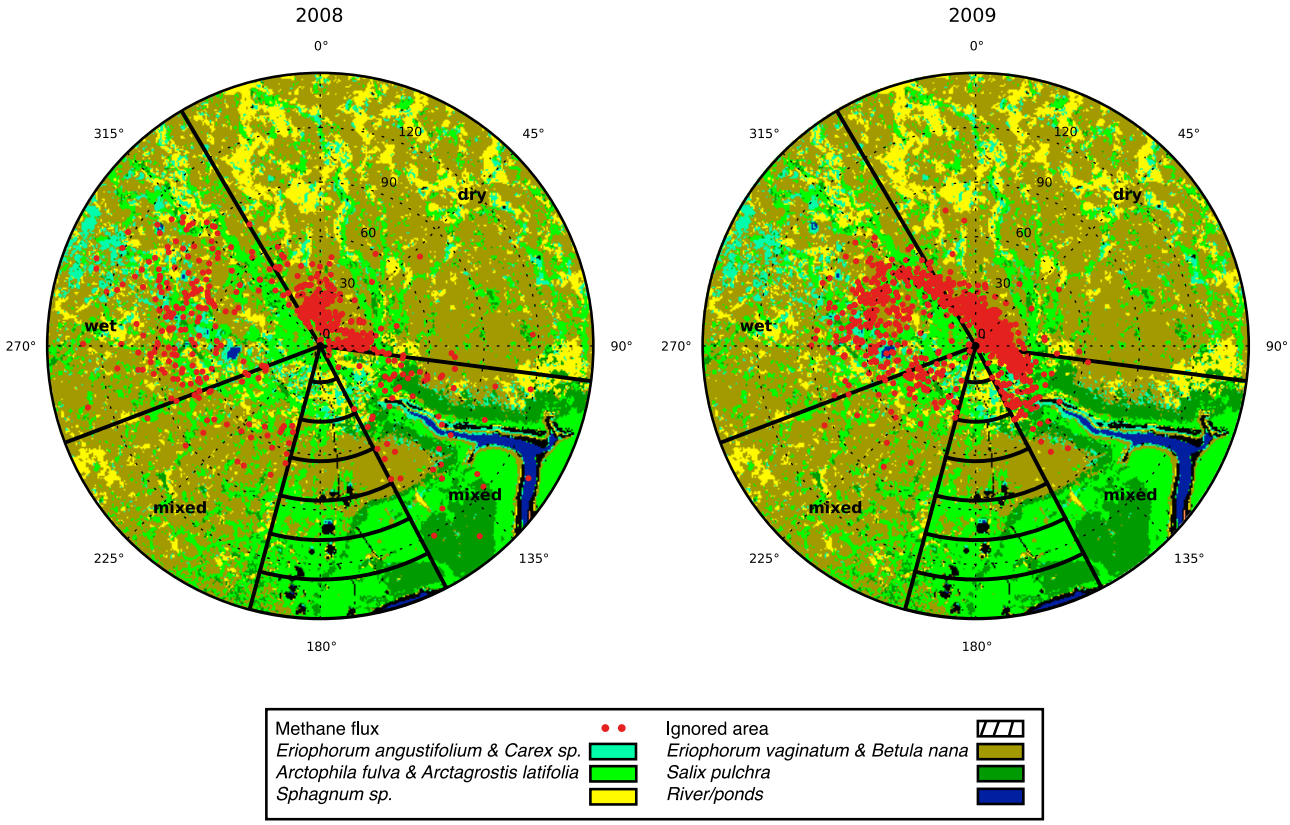

Figure 3. Half-hourly methane fluxes plotted against the wind direction on top of the satellite-derived vegetation map, which shows vegetation composition in a radius of 300 m around the tower. The tower is situated in the center, while the red points indicate the methane flux in (ϕ, r) coordinates where ϕ is wind direction and r is the flux magnitude in nmol CH_4 m^{-2} s^{-1}. The measurements are plotted along the wind direction, and the distance from the center indicates the size of the flux. Apart from wind direction, no further calculations on the source area are used in the plot. The dashed circles indicate the scale of the flux. The striped area indicates the direction from which data was discarded due to influence on the flux from the houses and the generator to the south (which are masked black in the map).

3.3. Diurnal Pattern

[30] In Figure 4, the diurnal pattern of methane flux, atmospheric stability and soil temperature are shown for 2008 and 2009, for the duration that the methane eddy covariance was run. Because of the large variation in amplitude between the three sectors, half-hourly measurements have been split up to show diurnal patterns for each sector separately. For each time of day, the average for the methane flux, atmospheric stability and soil temperature was determined for those measurements that were measured at that time and for the same sector. From this, the diurnal pattern of the various model parameters could be determined. Because of its low variation, water level was measured once a day and therefore not included in this graph.

[31] The data for the mixed sector in 2008 shows a large scatter since only a few data points were available for each time step, but for the other sectors enough data points were available to obtain a well averaged diurnal pattern. In all sectors and for all years, the methane flux shows a diurnal pattern, where methane fluxes are low during the night and

Table 1. Vegetation Composition for Three Wind Sectors According to Wetness, as Shown in Figure 3[a]

Sector	Dry (%)	Mixed (%)	Wet (%)	Methane Flux
Eriophorum angustifolium and *Carex* sp.	4	4	12	High to very high
Arctophila fulva and *Arctagrostis latifolia*	14	26	20	Average to high
Sphagnum sp.	19	8	14	Average
Eriophorum vaginatum and *Betula nana*	61	41	51	Low to none
Salix pulchra	2	18	3	Low to none
River/ponds	0	3	<1	Unknown/high
High-res image fractional pond cover	<1	<1	5	High

[a]Percentages are rounded. In the last column, it is shown how the different vegetation types compare relatively in terms of methane emission. Fluxes for the river are unknown; for ponds they are high. The fractional cover of the ponds, without the river, is shown in a second assessment with the use of a high-resolution (0.5 m) satellite image, which was able to capture small ponds better.

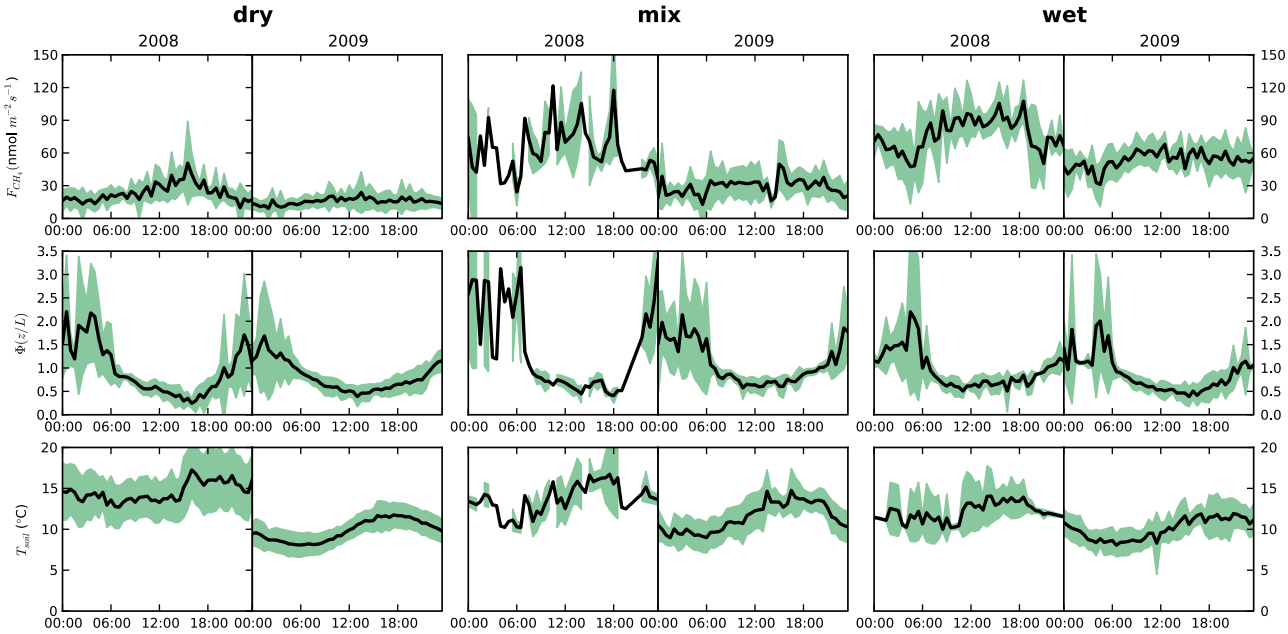

Figure 4. Diurnal patterns of methane flux, atmospheric stability, and soil temperature. The black line shows the average of half-hourly values, while the green shaded area shows standard deviations on these averages.

peak around 3 PM. When compared to the atmospheric stability, we see unstable conditions ($\Phi < 1$) during the day from 6 AM until 9 or 11 PM, followed by stable conditions ($\Phi > 1$) until 6 AM the next morning. The atmosphere is most unstable together with the peak in methane flux, around 3 PM, and methane fluxes are lower during stable atmospheric conditions. When compared to soil temperature, we see that it shows a very smooth diurnal pattern with a peak in temperature at the end of the afternoon, around 5 PM, and the lowest temperatures in the morning around 6 AM. In general, atmospheric stability shows an inverse relation to the methane flux while soil temperature lags behind on the peaks in methane flux.

3.4. Flux Model

[32] To prepare the data for model optimization, all observations under stable conditions where the stability function gave values higher than 5 were discarded, since the upwind area that contributes to the flux approaches infinite in these cases, which makes the eddy covariance method less representative [*Aubinet*, 2008]. Also, measurements where the wind was in the direction of the generator and the research station ($155° > \alpha < 195°$), were discarded since these observations were possibly disturbed. In 2008 this concerned 13% of the measurements while only 3% had to be discarded in 2009. Finally, to remove variations in the flux due to short-term changes in the footprint, all data for 2008 and 2009 was averaged over 3 h periods.

[33] After applying this data selection, the model was optimized separately for the three wind directions that showed distinctively different flux magnitudes as shown in Figure 3, due to their different compositions. Furthermore, the model was optimized with both the data of 2008 and 2009, to try to find parameter values that are applicable to both years. To allow for an unbiased calibration and validation, even days were used to calibrate the data and uneven days were used for validation. Scatterplots of stability, Φ, soil temperature, T_{soil}, and water level, w_l, against the observed fluxes are shown in Figure 5 and are split out according to the wind direction for the dry, mixed and wet sectors.

[34] The best fit for each parameter has been plotted in Figure 5, while Table 2 shows the values of the optimized model parameters for the three sectors. For each sector, a line depicts the modeled relationship with the environmental parameter. This line is drawn by separately plotting nonlinear relationships for each parameter, using the model parameters as shown in Table 2. For stability, the base parameters p_0 and p_1 were used to draw the relationship, while the nonlinear relationships with water level and soil temperature from equation (2) were ignored and the same procedure was applied to the other parameters. The correlation and the normalized root mean square deviation (NRMSD) between this fit and the observed fluxes are shown for each parameter. The NRMSD is an indicator of residual variance after comparing the model with the data. The lower the NRMSD, the better the model describes the observed data. The sum of the correlations in Figure 5 is larger than 1.0 for all of the three sectors, which suggests that the parameters also correlate with each other. This is true for water level and temperature: a higher water content in the soil increases its thermal conductivity [*Bristow et al.*, 2001], which leads to higher soil temperatures.

[35] The model did not significantly improve by adding additional nonlinear relationships from equation (2) with parameters such as wind speed, friction velocity or air pressure. Also, model performance did not change when soil temperature was replaced with air temperature or surface temperature calculated from long wave outgoing radiation. With the chosen parameters, the model performed well ($r^2 = 0.87$, NRMSD = 0.09) over the 2 years as shown

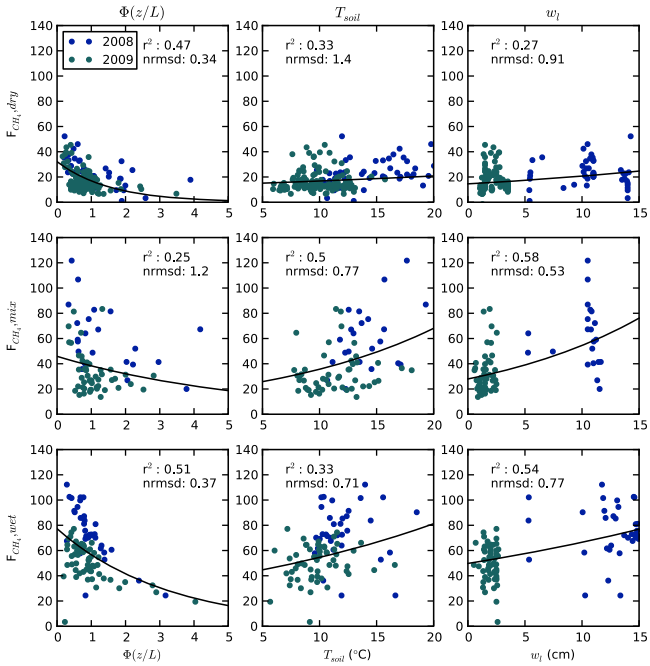

Figure 5. Environmental parameters plotted against observed methane fluxes. The columns show the parameters, $\Phi(z/L)$, T_{soil} and w_l, while the rows indicate the relationships for the three sectors that the model was optimized for (dry, mixed, and wet). Values for 2008 are shown in blue, while the measurements for 2009 are shown in grey. Methane fluxes are in nmol CH_4 m^{-2} s^{-1}.

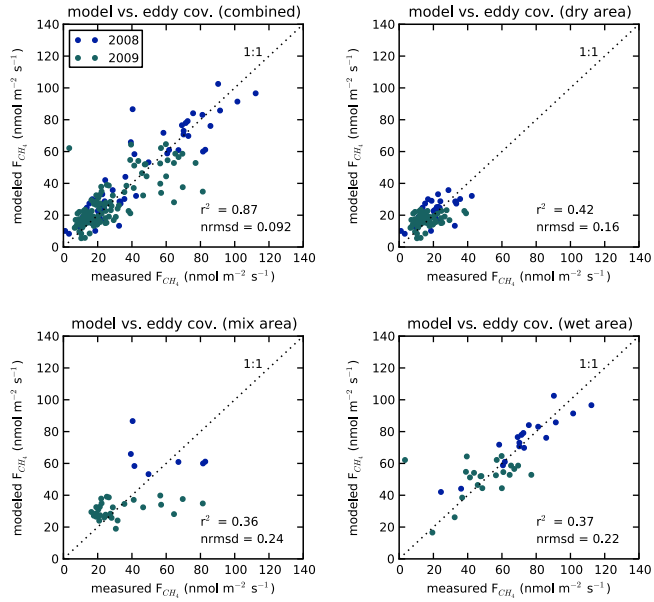

Figure 6. Observed versus measured fluxes. Model calibration has been performed on even days, and here model performances for uneven days are shown. The data has been split out to the dry, mixed, and wet sectors.

in Figure 6. Here model performance is plotted against the independent data set of the uneven days. Split out into the 2 years, the model and the data from 2008 showed a slightly better fit when compared to 2009 ($r^2 = 0.91$, NRMSD = 0.11 for 2008 and $r^2 = 0.72$, NRMSD = 0.14 for 2009). Figure 6 also shows the performance of the three submodels for the dry, mixed and wet sectors, which had a r^2 of 0.42, 0.36 and 0.37, respectively. The NRMSD was 0.16, 0.24 and 0.22 for the wet, mixed and dry sectors. Furthermore, a 1:1 line is plotted in Figure 6 to show the departure of the modeled values from the data.

[36] In Figure 7, the time series of fluxes and the model are shown as they changed throughout the season. Figure 7 shows that the model describes the temporal variation of the observed fluxes very well. In Figure 7, the model has also been run for the field campaign in 2007 and the period preceding the start of the eddy covariance in 2008. To validate the model for these periods, the modeled result has also been compared to flux chamber measurements that were performed in the vicinity of the tower in 2007, 2008 and 2009. This data was upscaled with the vegetation distribution of Table 1, along the dominant wind direction at the time of the flux measurement. Apart from the period following 26 July 2007, the chamber fluxes and the model show good agreement.

[37] While the model performs well to reproduce the observed fluxes, it has been constructed from the combined output of three submodels, as shown in Figure 7, and this provides a fragmented view of the emissions from the dry, mixed and wet sectors. To show the absolute difference in emissions from these areas, the cumulative methane fluxes of the combined model and its submodels are shown in Figure 8. From Figure 8 it becomes clear that the total emission of the wet sector is around 3 times higher than the emission of the dry sector, while the mixed sector shows around 2 to 2.5 times higher fluxes than the dry sector. This also follows from the values of the parameter p_0 in Table 2, which is 17.3, 38.6 and 57.3 for the dry, mixed and wet sectors, respectively. With an emission that is slightly below the average of the three sectors, the combined model fits in between. It is also suggested from Figure 8 that methane emissions were highest in 2007, somewhat lower in 2008 and at its lowest in 2009. However, the outcome of the model is tuned to data measured by the eddy covariance system, which varies with the wind direction. This means that chance determines how often a sector contributes to the overall flux and the model does not show the spatially averaged methane emission. To obtain a better estimate of the average methane flux emitted by the area within the footprint of the tower, the submodels for the three sectors have been averaged and weighted according to the radial size of the sector. Average fluxes are estimated to be 56.5, 48.7 and 30.4 nmol CH_4 m^{-2} s^{-1} for 2007, 2008 and 2009. The cumulative sum for one month (30 days), which is

Table 2. Values of the Model Parameters p0 to p4 of Equation (2) for the Three Submodels

Sector	p_0	p_1	p_2	p_3
Dry	17.3	0.53	1.24	1.04
Mixed	38.6	0.84	1.91	1.07
Wet	57.3	0.73	1.49	1.03

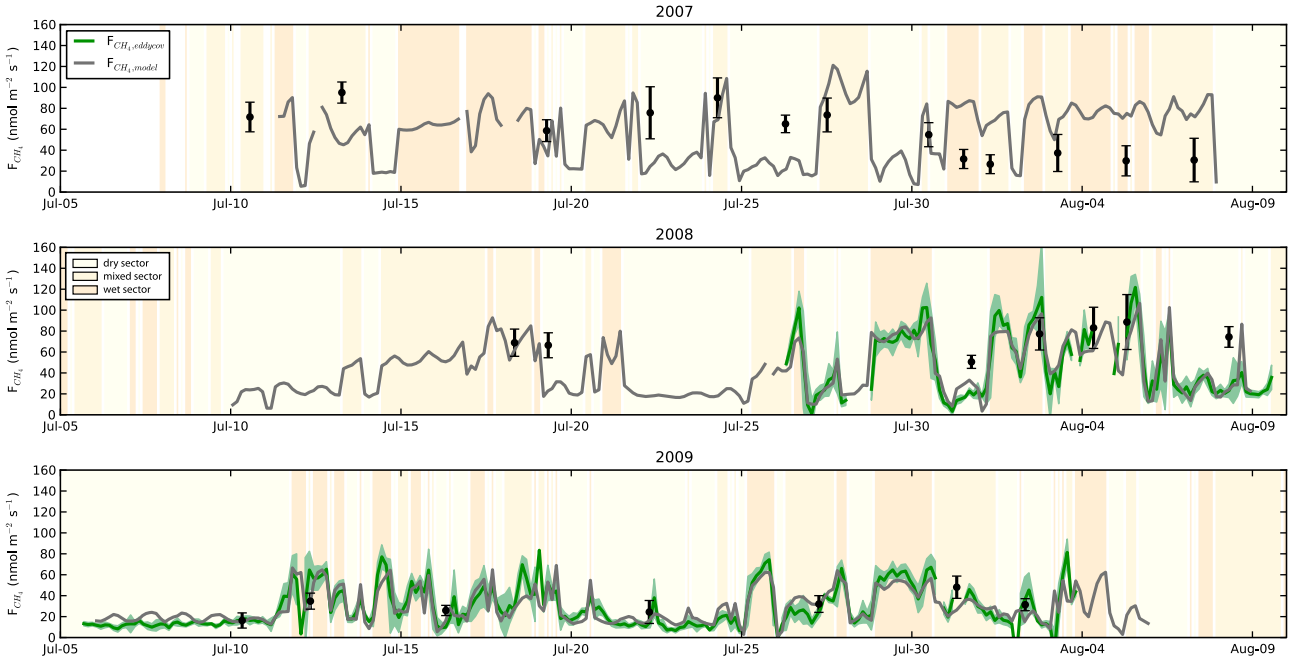

Figure 7. Methane fluxes as calculated with the chamber method (black error bars), eddy covariance (green line), and the model (grey line). The model and the eddy covariance are plotted in 3-hourly intervals. The green shaded region indicates the standard deviation of the measured flux within that period. The yellow background indicates the predominant wind direction for that period. Light yellow represents the dry sector, medium yellow represents the mixed sector, and the darker yellow represents the wet sector.

approximately the time scale depicted in Figure 8, was found to be 2.2 g CH_4 m^{-2} $month^{-1}$, 2.0 g CH_4 m^{-2} $month^{-1}$, and 1.3 g CH_4 m^{-2} $month^{-1}$ for the 3 years.

4. Discussion

4.1. Eddy Covariance Measurements

[38] In this study, the methane fluxes measured by the eddy covariance setup were shown to be highly variable and exhibited distinctively different magnitudes between years. In Figure 2, the conditions for all measurement years are shown and it is obvious that water level, temperature and, as a result, methane fluxes were higher in 2008, compared to 2009. Also, because of the higher temperatures, active layer depth was larger in 2008 than in 2009. Contrary to these long-term differences, the underlying causes of the short-term changes in methane fluxes are not immediately clear from Figure 2. However, Figure 3 clearly shows that methane fluxes differed with a change in wind direction and thus in source area. The area to the south and the west was wetter and had a vegetation composition with a higher sedge vegetation cover. Since this vegetation type shows the highest

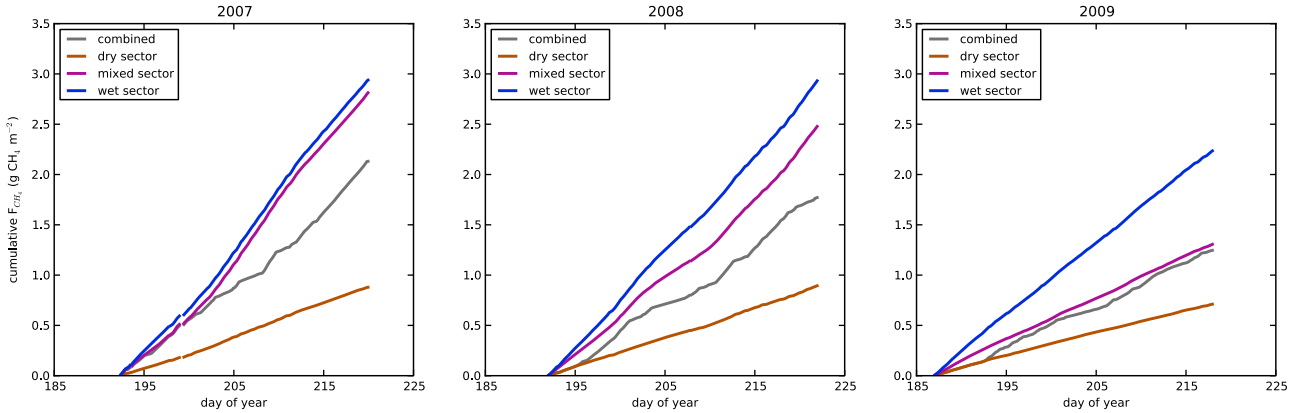

Figure 8. Cumulative plots of the model versus the day of year for 2007, 2008, and 2009. The grey line shows the cumulative flux of the model as it was plotted in Figure 6, with different model parameters with varying wind direction. The other lines show the cumulative plots of the submodels for the dry (brown), mixed (purple), and wet (blue) sectors.

methane fluxes [*van Huissteden et al.*, 2005], it is not surprising that fluxes measured at the eddy covariance tower were higher when the predominant wind was blowing from these directions. From these two directions, fluxes were even higher for westerly winds, since that sector included a higher number of ponds, associated with high methane fluxes [*Bastviken et al.*, 2004; *Walter et al.*, 2006] and higher amounts of wet vegetation as shown in Table 1. The area to the northwest was much dryer with less sedge vegetation and almost no ponds, resulting in much lower fluxes compared to the other wind directions.

[39] These changes in fetch made it difficult to ascertain whether fluxes showed a diurnal pattern but by splitting the data up in the three sectors and arranging them according to the time of day, a plot of diurnal patterns could be made as shown in Figure 4. In Figure 4, it was shown that atmospheric stability and methane flux showed an inverse relation, with higher fluxes under unstable conditions during daytime, and lower fluxes under stable conditions during nighttime. At the same time, soil temperature also showed a clear diurnal pattern but peaks in soil temperature were mostly seen after the peak in methane flux occurred. This would suggest that the effect of soil temperature on methane fluxes is obscured by the effect of atmospheric stability, which has been observed before for eddy covariance measurements of CO_2 [*Hollinger et al.*, 1998]. Under unstable conditions, air parcels close to the ground are warmer and this increases buoyancy and vertical transport of air, including methane. During stable conditions, air parcels close to the ground are colder and vertical transport is constrained, damping methane fluxes. In these periods, higher methane concentrations were observed regularly at the tower, indicating a buildup of methane. While previous studies considered mostly daily values, this study uses smaller time scales and as such the diurnal effect of atmospheric stability on vertical transport has to be taken into account.

4.2. Flux Model Performance

[40] Following the interpretation of the measurements, atmospheric stability, soil temperature and water level were used as parameters to the model. In Figure 6, the model results have been plotted against the eddy covariance measurements, along with the correlation and NRMSD. From the correlations and the NRMSD, we see that the combined model simulated the observed fluxes well (r^2 = 0.87, NRMSD = 0.09) and they show a good 1:1 linear agreement. For the components of the model, the dry sector is modeled best (r^2 = 0.42, NRMSD = 0.16), while the mixed and wet sector are modeled less well (r^2 = 0.36 and 0.37, NRMSD = 0.24 and 0.22 respectively). These model performances are reasonable, considering that each sector holds many different vegetation types that are not uniformly distributed, which causes variation in the signal when the fetch within a sector changes. This perhaps explains the larger spread between model and data for the mixed sector. This variability in the data is not explained by the model and is possibly due to footprint changes. Arguably, this scatter could be addressed by calculating the different contributions of each vegetation type with the use of the footprint model and the satellite-derived vegetation map. However, footprint calculations have a high uncertainty of their own and it is not ensured that their application would improve model accuracy. Also, by splitting up the model in even smaller footprint areas, the amount of data available for calibration would be reduced, which would complicate robust model optimization. By dividing the area in a limited number of sectors, it is ensured that the model remains simple, while achieving acceptable performance.

[41] The correlations and the NRMSD show that atmospheric stability explained most of the variation observed in the dry and wet sector (r^2 = 0.47 and 0.51, NRMSD = 0.34 and 0.37, respectively) while it was a poor predictor in the mixed sector (r^2 = 0.25, NRMSD = 1.2). Soil temperature was a poor predictor in the dry sector but explained part of the variation in the mixed and wet sector (r^2 = 0.5 and 0.33, NRSMD = 0.77 and 0.71). Finally, water level was the best predictor to observed variations in the mixed sector (r^2 = 0.58, NRMSD = 0.53), while only part of the variation in the dry and wet sector was explained by water level (r^2 = 0.27 and 0.54, NRSMD = 0.91 and 0.77). The strong relation with water level in the mixed sector can be explained by its vegetation distribution and topography. This area shows gentle small-scale topographic differences and as such, a small increase in the water level leads to a large increase in flooded areas and thus in methane fluxes. This has also been observed in the field: the extent of inundated areas was much lower in 2009 than in 2008, which is also represented by the partitioning of the fluxes for these years along water level. Water level also partly explained the variation in the wet sector, but due to the higher amount of ponds, whose areal size is less sensitive to water level changes, the residuals from fitting this parameter were higher. In the dry sector, it seems that no strong relationship with water level exists, which can be explained by the already low amount of wet areas in this sector.

4.3. Alternative Parameter Selection

[42] Previous studies on eddy covariance measurements of methane fluxes have found relationships with various parameters such as mean wind speed [*Fan et al.*, 1992], temperature, water level [*Suyker et al.*, 1996], active layer depth [*Friborg et al.*, 2000], friction velocity [*Wille et al.*, 2008] and air pressure [*Sachs et al.*, 2008]. Not all of the these relationships were found in the current study, which is possibly due to the use of 3 h averages. Although some have sought to explain the diurnal variation [*Zona et al.*, 2009], most previous studies sought relationships with daily averaged values. This study provides a framework for a higher temporal resolution but this may lead to different relationships with environmental parameters.

[43] In some of the previous studies wind speed and friction velocity were shown to increase methane emissions from open water and therefore we tested model performance when wind speed or friction velocity were used, while leaving atmospheric stability out of the equation. The resulting fits of friction velocity and wind speed against methane fluxes showed low correlations (typically around 0.2) and a high NRMSD of 2 or 3. Also, optimizations for the three sectors differed where some fits showed an increase in fluxes with higher friction velocity or wind speed, while others showed opposite fits. Actually, the model performed better when friction velocity and wind speed were left out of the equation, which was also indicated by the high NRMSD values. Apparently, friction velocity and wind speed were not suitable

Table 3. Comparison of Summer Eddy Covariance Measurements of Methane From Various (Sub) Arctic Sites

Region	Site	Vegetation	Average flux (nmol CH_4 m^{-2} s^{-1})	References
Alaska	Bethel	Dry upland tundra	7.9 ± 2	*Fan et al.* [1992]
Alaska	Bethel	Wet meadow tundra	20.9 ± 2	*Fan et al.* [1992]
Alaska	Barrow	Wet sedge tundra	17.7	*Zona et al.* [2009]
Greenland	Zackenberg	High Arctic fen	7.2–86.6	*Friborg et al.* [2000]
Sweden	Stordalen	Subarctic mire	107.4 ± 45.0	*Jackowicz-Korczyński et al.* [2010]
Siberia	Lena Delta	Wet polygonal tundra	11.0–16.1	*Wille et al.* [2008]; *Sachs et al.* [2008]
Siberia	Chokurdakh	Mixed moist tundra	30.4–56.5	This study

to explain fluxes on this high resolution and they were therefore not used in the model equation.

[44] Also, model results did not improve when air pressure was added. It has been established that air pressure has a direct effect on ebullition from peatlands [*Kellner et al.*, 2006] and it has since been used to explain variations in tundra methane fluxes as measured by eddy covariance [*Sachs et al.*, 2008]. However, in this model the effect of air pressure was not pronounced. By adding air pressure, the r^2 of the model improved slightly by 0.01 points, mostly because of a slightly better fit for the dry sector. On the other hand, model performance became much worse for the mixed sector. The optimization with air pressure resulted in a poor fit for temperature with a slope near to zero. For the wet sector, a marginal relationship was found with air pressure, which did not influence the model result. Because of these varying responses to air pressure and its low contribution to improving the model, it was decided to exclude air pressure from the model.

[45] This lack of a relationship with air pressure might be explained by the soil conditions at the site. Air pressure effects ebullition but for large pulses to occur, a lot of methane has to be built up in the soil. This would require a large reservoir for methane while at this site the peat layer is only 15 cm thick, underlain by compact silt and the active layer reaches a maximum of just 30 to 50 cm. This provides for limited space where methane can accumulate, which is required to see significant pulses of methane when air pressure drops. Also, the division of fluxes into the three wind directions could further explain the poor fit with air pressure. Air pressure changes occur at time scales of several days, while a limited amount of measurement days were available per sector. More measurements, with a larger variation in air pressure for all wind directions, might lead to an improved understanding of air pressure effects on the measured fluxes.

[46] Apart from wind speed, turbulence and air pressure, another parameter that was not included in the parameter set, was active layer depth. Active layer depth can be used to model methane fluxes as shown by *Friborg et al.* [2000] and fluxes at a small plot scale showed differences along active layer depth at this site [*van Huissteden et al.*, 2005]. As can be seen in Figure 2, the temporal variation of the active layer was quite low, with a slow increase during the season. The largest difference in active layer was between the 2 measurement years, similar to the relationship with water level and a good model fit for active layer depth would thus result in a poor fit with water level, or vice versa. Besides, a deeper active layer would lead to higher fluxes in the model and the very deep active layer in 2007 would thus translate into a higher amplitude of the modeled flux for that year. Since the model already simulated fluxes for August 2007 that were higher than measurements performed with the independent flux chambers, this overestimation would only be increased by adding active layer depth. Therefore, active layer depth was not included in the model.

4.4. Comparison With Chamber Fluxes and Extension of the Model

[47] To compare the eddy covariance and the model with an independent technique, measured and modeled fluxes were also plotted with simultaneously performed flux chamber measurements in Figure 7. These flux measurements were upscaled according to the vegetation composition of the sector for the wind direction at the time of measurement. For both 2008 and 2009, chamber fluxes mostly agree with the eddy covariance measurements. Figure 7 shows the results from the model, which in 2008 and 2009 shows good agreement with the chamber measurements and the eddy covariance.

[48] Because of the good agreement between the model and the chamber flux measurements, it was decided to apply the model to the fieldwork period of 2007. In that year methane fluxes were measured just with the chamber flux technique but the number of flux measurements was higher than in 2008 and 2009, allowing for good comparison. Figure 7 shows that the model and the chamber fluxes agree quite well for the month of July but that in August modeled fluxes are much higher than the upscaled chamber fluxes. As can be seen from Figure 2, soil temperatures lowered at the start of August, which led to lower methane fluxes. Apparently the measured chamber fluxes in 2007 were more sensitive to a lowering of soil temperature than the model would suggest. In 2007, the soil thermal regime was very different from the other years, since the start of the growing season was much earlier and this led to a much thicker active layer. Because the model was calibrated to years with a shallower active layer depth, the different soil conditions could provide an explanation for the poor agreement between the chamber flux measurements and the model. Although care has to be taken when the model is applied to years with highly different environmental conditions, the model agreed well for the majority of the measurements in 2007.

[49] With the addition of the model runs for the periods without eddy covariance measurements, estimates of average fluxes for the summer fieldwork seasons of 2007, 2008 and 2009 can be made. By using the average of the three submodels, in proportion to the size of each sector, average methane fluxes were estimated at 56.5, 48.7 and 30.4 nmol CH_4 m^{-2} s^{-1} for 2007, 2008 and 2009, respectively. Compared to other eddy covariance studies on methane from

around the Arctic, as shown in Table 3, this site exhibits methane emission rates amongst the highest reported.

5. Conclusion

[50] In this study, the eddy covariance technique was used to measure methane fluxes at a tundra site in northeastern Siberia. These fluxes showed to be highly variable, with large changes occurring within hours. From a careful data analysis, most of these variations could be explained by a change in fetch, atmospheric stability, soil temperature and water level. After splitting the data into three sectors, according to their degree of wetness, these parameters were used to calibrate a nonlinear model, which successfully reproduced the observed fluxes. Model performance did not significantly improve by the addition of air pressure, active layer depth, wind speed or friction velocity. This is possibly due to the higher temporal resolution and the limited amount of measurement days per sector.

[51] Since the model was optimized on measurements from 2 separate years, the underlying causes of the inter-annual variation in fluxes could be well defined. These differences were explained mostly by water level, followed by soil temperature. Following these relationships, the model was extended outside of the calibrated period and compared to independent flux chamber measurements. Although some discrepancies were noted between the flux chamber measurements and the model, overall the two methods compared well. From the output of the model, it was derived that the average summer fluxes for 2007, 2008 and 2009 were 56.5, 48.7 and 30.4 nmol CH_4 m^{-2} s^{-1}, respectively. These values are amongst the highest reported when compared to other sites across the Arctic.

[52] Although previous studies have measured within-day variation in methane fluxes as measured by eddy covariance, to our knowledge there are currently no studies that have provided a method to model fluxes at such short time steps. Because of the short time step of the presented method, it makes it ideal for gap-filling methane flux data, of which currently few alternatives are available. Also, if the model parameterization has been performed on a data set that shows enough spread in variation between and within years, the model can be used to estimate methane fluxes for other years as well.

[53] This study also showed that the measurements performed with the eddy covariance method were very dependent on changes in the wind direction and the associated source area. These changes in fetch led to a fragmented measurement of methane fluxes of the area. This problem could successfully be accounted for by tuning the model separately for each source area. Subsequently, these sub-models could be used to determine the spatially averaged emissions despite the highly heterogenous terrain. However, when performing eddy covariance measurements of methane within an area that shows these kinds of large differences in water level and areal extent of ponds, preferably the use of more than one tower is needed to determine spatially integrated methane emissions more accurately.

[54] **Acknowledgments.** We would like to acknowledge the people at the Institute for Biological Problems of the Cryolithozone SB RAS in Yakutsk for their assistance in and outside the field, especially Alexander V. Kononov for all the help with the import of equipment in 2008. Also, we would like to thank T. G. Strukova and the rangers of the Kytalyk Resource Reserve for their logistical support to and from the site and other assistance. Furthermore, we would like to acknowledge the people from the engineering and electronics workshop at the VU University Amsterdam, especially Rob Stoevelaar and Ron Lootens, without whom the successful installation of the eddy covariance equipment would not have been possible. We want to acknowledge the Darwin Center for Biogeosciences who supported this research with a grant to F. J. W. Parmentier (142.16.1041). Additional funding for successful completion of this research was provided by the NWO Dutch Russian research cooperation programme entitled "Long term observation of soil carbon and methane fluxes in Siberian tundra" (047.017.037) and the GreenCyclesII training network (7th Framework programme reference 238366).

References

Aubinet, M. (2008), Eddy covariance CO_2 flux measurements in nocturnal conditions: An analysis of the problem, *Ecol. Appl.*, *18*(6), 1368–1378.

Aubinet, M., et al. (2000), Estimates of the annual net carbon and water exchange of forests: The EUROFLUX methodology, *Adv. Ecol. Res.*, *30*, 113–175.

Bastviken, D., J. Cole, M. Pace, and L. Tranvik (2004), Methane emissions from lakes: Dependence of lake characteristics, two regional assessments, and a global estimate, *Global Biogeochem. Cycles*, *18*, GB4009, doi:10.1029/2004GB002238.

Bristow, K. L., G. J. Kluitenberg, C. J. Goding, and T. S. Fitzgerald (2001), A small multi-needle probe for measuring soil thermal properties, water content and electrical conductivity, *Comput. Electr. Agric.*, *31*(3), 265–280.

Bubier, J. L. (1995), The relationship of vegetation to methane emission and hydrochemical gradients in northern peatlands, *J. Ecol.*, *83*(3), 403–420.

Christensen, T. R., S. Jonasson, T. V. Callaghan, and M. Havstrom (1995), Spatial variation in high-latitude methane flux along a transect across Siberian and European tundra environments, *J. Geophys. Res.*, *100*(D10), 21,035–21,045.

Christensen, T. R., T. Johansson, H. J. Åkerman, M. Mastepanov, N. Malmer, T. Friborg, P. Crill, and B. H. Svensson (2004), Thawing sub-arctic permafrost: Effects on vegetation and methane emissions, *Geophys. Res. Lett.*, *31*, L04501, doi:10.1029/2003GL018680.

Corradi, C., O. Kolle, K. M. Walter, S. A. Zimov, and E.-D. Schulze (2005), Carbon dioxide and methane exchange of a north-east Siberian tussock tundra, *Global Change Biol.*, *11*(11), 1910–1925.

Denmead, O. T. (2008), Approaches to measuring fluxes of methane and nitrous oxide between landscapes and the atmosphere, *Plant Soil*, *309*(1–2), 5–24.

Dorrepaal, E., S. Toet, R. S. P. van Logtestijn, E. Swart, M. J. van de Weg, T. V. Callaghan, and R. Aerts (2009), Carbon respiration from subsurface peat accelerated by climate warming in the subarctic, *Nature*, *460*(7255), 616–619.

Fan, S. M., S. C. Wofsy, P. S. Bakwin, D. J. Jacob, S. M. Anderson, P. L. Kebabian, J. B. McManus, C. E. Kolb, and D. R. Fitzjarrald (1992), Micrometeorological measurements of CH_4 and CO_2 exchange between the atmosphere and sub-arctic tundra, *J. Geophys. Res.*, *97*(D15), 16,627–16,643.

Friborg, T., T. R. Christensen, B. U. Hansen, C. Nordstroem, and H. Soegaard (2000), Trace gas exchange in a high-Arctic valley: 2. Landscape CH_4 fluxes measured and modeled using eddy correlation data, *Global Biogeochem. Cycles*, *14*(3), 715–723.

Hendriks, D. M. D., A. J. Dolman, M. K. van der Molen, and J. van Huissteden (2008), A compact and stable eddy covariance set-up for methane measurements using off-axis integrated cavity output spectroscopy, *Atmos. Chem. Phys.*, *8*(2), 431–443.

Hollinger, D., et al. (1998), Forest-atmosphere carbon dioxide exchange in eastern Siberia, *Agric. For. Meteorol.*, *90*(4), 291–306.

Jackowicz-Korczyński, M., T. R. Christensen, K. Bäckstrand, P. Crill, T. Friborg, M. Mastepanov, and L. Ström (2010), Annual cycle of methane emission from a subarctic peatland, *J. Geophys. Res.*, *115*, G02009, doi:10.1029/2008JG000913.

Kaufman, D. S., et al. (2009), Recent warming reverses long-term Arctic cooling, *Science*, *325*(5945), 1236–1239.

Kellner, E., A. J. Baird, M. Oosterwoud, K. Harrison, and J. M. Waddington (2006), Effect of temperature and atmospheric pressure on methane (CH_4) ebullition from near-surface peats, *Geophys. Res. Lett.*, *33*, L18405, doi:10.1029/2006GL027509.

Kormann, R., and F. X. Meixner (2001), An analytical footprint model for non-neutral stratification, *Boundary Layer Meteorol.*, *99*(2), 207–224.

Kutzbach, L., C. Wille, and E.-M. Pfeiffer (2007), The exchange of carbon dioxide between wet Arctic tundra and the atmosphere at the Lena River Delta, northern Siberia, *Biogeosciences*, *4*(5), 869–890.

Levenberg, K. (1944), A method for the solution of certain non-linear problems in least squares, *Q. Appl. Math.*, *2*, 164–168.

Mastepanov, M., C. Sigsgaard, E. J. Dlugokencky, S. Houweling, L. Ström, M. P. Tamstorf, and T. R. Christensen (2008), Large tundra methane burst during onset of freezing, *Nature*, *456*(7222), 628–630.

McGuire, A. D., et al. (2009), Sensitivity of the carbon cycle in the Arctic to climate change, *Ecol. Monogr.*, *79*(4), 523–555.

Moncrieff, J. B., et al. (1997), A system to measure surface fluxes of momentum, sensible heat, water vapour and carbon dioxide, *J. Hydrol.*, *189*(1–4), 589–611.

Moore, C. J. (1986), Frequency-response corrections for eddy-correlation systems, *Boundary Layer Meteorol.*, *37*(1–2), 17–35.

Morrissey, L. A., D. B. Zobel, and G. P. Livingston (1993), Significance of stomatal control on methane release from carex-dominated wetlands, *Chemosphere*, *26*(1–4), 339–355.

Nakai, T., M. K. van der Molen, J. H. C. Gash, and Y. Kodama (2006), Correction of sonic anemometer angle of attack errors, *Agric. For. Meteorol.*, *136*(1–2), 19–30.

Nakano, T., S. Kuniyoshi, and M. Fukuda (2000), Temporal variation in methane emission from tundra wetlands in a permafrost area, northeastern Siberia, *Atmos. Environ.*, *34*(8), 1205–1213.

Oechel, W. C., S. J. Hastings, G. L. Vourlitis, M. Jenkins, G. Riechers, and N. Grulke (1993), Recent change of Arctic tundra ecosystems from a net carbon-dioxide sink to a source, *Nature*, *361*(6412), 520–523.

Oechel, W. C., G. L. Vourlitis, S. Brooks, T. L. Crawford, and E. Dumas (1998), Intercomparison among chamber, tower, and aircraft net CO_2 and energy fluxes measured during the Arctic System Science Land-Atmosphere-Ice Interactions (ARCSS-LAII) Flux Study, *J. Geophys. Res.*, *103*(D22), 28,993–29,003.

Paulson, C. A. (1970), The mathematical representation of wind speed and temperature profiles in the unstable atmospheric surface layer, *J. Appl. Meteorol.*, *9*(6), 857–861.

Sachs, T., C. Wille, J. Boike, and L. Kutzbach (2008), Environmental controls on ecosystem-scale CH_4 emission from polygonal tundra in the Lena River Delta, Siberia, *J. Geophys. Res.*, *113*, G00A03, doi:10.1029/2007JG000505.

Schuur, E. A. G., et al. (2008), Vulnerability of permafrost carbon to climate change: Implications for the global carbon cycle, *Bioscience*, *58*(8), 701–714.

Serreze, M. C., et al. (2000), Observational evidence of recent change in the northern high-latitude environment, *Clim. Change*, *46*(1–2), 159–207.

Suyker, A. E., S. B. Verma, R. J. Clement, and D. P. Billesbach (1996), Methane flux in a boreal fen: Season-long measurement by eddy correlation, *J. Geophys. Res.*, *101*(D22), 28,637–28,647.

Torn, M. S., and F. S. Chapin III (1993), Environmental and biotic controls over methane flux from Arctic tundra, *Chemosphere*, *26*(1–4), 357–368.

van der Molen, M. K., J. H. C. Gash, and J. A. Elbers (2004), Sonic anemometer (co)sine response and flux measurement—II. The effect of introducing an angle of attack dependent calibration, *Agric. For. Meteorol.*, *122*(1–2), 95–109.

van der Molen, M. K., M. J. Zeeman, J. Lebis, and A. J. Dolman (2006), EClog: A handheld eddy covariance logging system, *Comput. Electr. Agric.*, *51*(1–2), 110–114.

van der Molen, M. K., J. van Huissteden, F. J. W. Parmentier, A. M. R. Petrescu, A. J. Dolman, T. C. Maximov, A. V. Kononov, S. V. Karsanaev, and D. A. Suzdalov (2007), The growing season greenhouse gas balance of a continental tundra site in the Indigirka lowlands, NE Siberia, *Biogeosciences*, *4*(6), 985–1003.

van Huissteden, J., T. C. Maximov, and A. J. Dolman (2005), High methane flux from an Arctic floodplain (Indigirka lowlands, eastern Siberia), *J. Geophys. Res.*, *110*, G02002, doi:10.1029/2005JG000010.

Verma, S. B., F. G. Ullman, D. Billesbach, R. J. Clement, J. Kim, and E. S. Verry (1992), Eddy-correlation measurements of methane flux in a northern peatland ecosystem, *Boundary Layer Meteorol.*, *58*(3), 289–304.

Vourlitis, G. L., and W. C. Oechel (1997), Landscape-scale CO_2, H_2O vapour and energy flux of moist-wet coastal tundra ecosystems over two growing seasons, *J. Ecol.*, *85*(5), 575–590.

Walter, K. M., S. A. Zimov, J. P. Chanton, D. Verbyla, and F. S. Chapin III (2006), Methane bubbling from Siberian thaw lakes as a positive feedback to climate warming, *Nature*, *443*(7107), 71–75.

Webb, E. K., G. I. Pearman, and R. Leuning (1980), Correction of flux measurements for density effects due to heat and water vapour transfer, *Q. J. R. Meteorol. Soc.*, *106*(447), 85–100.

Whalen, S. C., and W. S. Reeburgh (1990), Consumption of atmospheric methane by tundra soils, *Nature*, *346*(6280), 160–162.

Wille, C., L. Kutzbach, T. Sachs, D. Wagner, and E.-M. Pfeiffer (2008), Methane emission from Siberian Arctic polygonal tundra: Eddy covariance measurements and modeling, *Global Change Biol.*, *14*(6), 1395–1408.

Zahniser, M. S., D. D. Nelson, J. B. McManus, and P. L. Kebabian (1995), Measurement of trace gas fluxes using tunable diode-laser spectroscopy, *Philos. Trans. R. Soc. London, Ser. A*, *351*(1696), 371–381.

Zona, D., W. C. Oechel, J. Kochendorfer, K. T. Paw U, A. N. Salyuk, P. C. Olivas, S. F. Oberbauer, and D. A. Lipson (2009), Methane fluxes during the initiation of a large-scale water table manipulation experiment in the Alaskan Arctic tundra, *Global Biogeochem. Cycles*, *23*, GB2013, doi:10.1029/2009GB003487.

A. J. Dolman and J. van Huissteden, Department of Hydrology and Geo-environmental Sciences, Faculty of Earth and Life Sciences, VU University Amsterdam, de Boelelaan 1085, NL-1081 HV, Amsterdam, Netherlands.

S. A. Karsanaev and T. C. Maximov, BioGeochemical Cycles of Permafrost Ecosystems Lab, Institute for Biological Problems of the Cryolithozone SB RAS, Lenin Ave. 41, 677980, Yakutsk, Russia.

F. J. W. Parmentier, Division of Physical Geography and Ecosystems Analysis, Department of Earth and Ecosystem Sciences, Lund University, Sölvegatan 12, SE-223 62 Lund, Sweden. (frans-jan.parmentier@nateko.lu.se)

G. Schaepman-Strub, Institute of Evolutionary Biology and Environmental Studies, University of Zürich, Winterthurerstr. 190, CH-8057, Zürich, Switzerland.

M. K. van der Molen, Meteorology and Air Quality Group, Wageningen University, Droevendaalsesteeg 4, NL-6708 PB, Wageningen, Netherlands.